Title

Selective Automated Perimetry Under Photopic, Mesopic, and Scotopic Conditions: Detection Mechanisms and Testing Strategies.

Journal

Translational Vision Science and Technology, 5(3)

ISSN

2164-2591

Authors

MacLaren, Robert
Simunovic, Matthew
Moore, Anthony

Publication Date

2016-05-01

DOI

10.1167/tvst.5.3.10

Peer reviewed

tvst

DOI: 10.1167/tvst.5.3.10

Article

Selective Automated Perimetry Under Photopic, Mesopic, and Scotopic Conditions: Detection Mechanisms and Testing Strategies

Matthew P. Simunovic[1,2,3,4], Anthony T. Moore[5,6,7], and Robert E. MacLaren[1,2,6]

[1] Nuffield Laboratory of Ophthalmology, Nuffield Department of Clinical Neurosciences, University of Oxford, Oxford OX3 9DU, UK
[2] Oxford Eye Hospital, Oxford University Hospitals NHS Trust, Oxford OX3 9DU, UK
[3] Save Sight Institute, University of Sydney, 8 Macquarie St., Sydney, NSW 2000, Australia
[4] Retinal Unit, Sydney Eye Hospital, 8 Macquarie Street, Sydney, NSW 2000, Australia
[5] Department of Ophthalmology, University of California San Francisco, 533 Parnassus Avenue, San Francisco, CA, USA
[6] Moorfields Eye Hospital, 162 City Road, London EC1V 2PD, UK
[7] Institute of Ophthalmology, University College London, 11-43 Bath Street, London EC1V 9EL, UK

Correspondence: Matthew P. Simunovic, Nuffield Laboratory of Ophthalmology, Nuffield Department of Clinical Neurosciences, University of Oxford, Oxford OX3 9DU, UK. e-mail: mps23@cantab.net

Received: 2 December 2015
Accepted: 2 March 2016
Published: 20 May 2016

Keywords: rod perimetry; cone perimetry; selective perimetry; mesopic perimetry; photopic perimetry

Citation: Simunovic MP, Moore AT, MacLaren RT. Selective automated perimetry under photopic, mesopic, and scotopic conditions: detection mechanisms and testing strategies. Trans Vis Sci Tech. 2016;5(3):10, doi: 10.1167/tvst.5.3.10

Purpose: Automated scotopic, mesopic, and photopic perimetry are likely to be important paradigms in the assessment of emerging treatments of retinal diseases, yet our knowledge of the photoreceptor mechanisms detecting targets under these conditions remains largely dependent on simian data. We therefore aimed to establish the photoreceptor/postreceptoral mechanisms detecting perimetric targets in humans under photopic, mesopic, and scotopic conditions and to make recommendations for suitable clinical testing strategies for selective perimetry.

Methods: Perimetric sensitivities within 30° of fixation were determined for eight wavelengths (410, 440, 480, 520, 560, 600, 640, and 680 nm) under scotopic, mesopic (1.3 cd.m^{-2}) and photopic (10 cd.m^{-2}) conditions. Data were fitted with vector combinations of rod, S-cone, nonopponent M+L-cone mechanism, and opponent M- versus L-cone mechanism templates.

Results: Scotopicperimetric sensitivity was determined by rods peripherally and by a combination of rods and cones at, and immediately around, fixation. Mesopic perimetric sensitivity was mediated by M+L-cones and S-cones centrally and by M+L-cones and rods more peripherally. Photopic perimetric sensitivity was determined by an opponent M- versus L-cone, a nonopponent M+L-cone, and an S-cone mechanism centrally and by a combination of an S-cone and an M+L-cone mechanism peripherally.

Conclusions: Under scotopic conditions, a 480-nm stimulus provides adequate isolation ($\geq$28 dB) of the rod mechanism. Several mechanisms contribute to mesopic sensitivity: this redundancy in detection may cause both insensitivity to broadband white targets and ambiguity in determining which mechanism is being probed with short-wavelength stimuli. M- and L-cone–derived mechanisms are well isolated at 10 cd.m^{-2}: these may be selectively probed by a stimulus at 640 nm ($\geq$ 20 dB isolation).

Translation Relevance: In human observers, multiple mechanisms contribute to the detection of Goldmann size III and size V perimetric targets under scotopic, mesopic, and photopic conditions. The relative contribution of these mechanisms appears to differ from those found previously for macaques. Our results furthermore suggest that caution must be exercised when using microperimetric techniques, which are typically conducted under mesopic conditions and which are likely to be important in the assessment of emerging treatments for retinal disease. This is because mesopic background conditions maximize the redundancy of target detection. Furthermore, our results demonstrate that spectral manipulation of the stimulus alone cannot be used to reliably separate rod from cone responses under these conditions.

Introduction

Clinical perimetry probes photopic or mesopic threshold sensitivity and typically employs broadband white adapting backgrounds of 10 or 1.3 cd.m^{-2}, respectively.[1] While most modern computerized perimeters use 10 cd.m^{-2} broadband white backgrounds, several newer instruments, in particular those that combine scanning laser ophthalmoscopy with perimetry (so-called "microperimeters"), use 1.3 cd.m^{-2} backgrounds.[2] Microperimeters provide a means of studying the structure–function relationship in retinal disease[2] and are likely to prove pivotal in studies of emerging treatments, such as gene[3] and stem cell therapies. Similarly, selective perimetric techniques, which seek to distinguish rod from cone responses under scotopic and photopic conditions,[4] are likely to be important in studies of emerging treatments. Such techniques are ideal because they offer the potential of identifying isolated or preferential loss of photoreceptor classes. Furthermore, they are paradigms that reduce the "redundancy" of target detection: it has been proposed that this feature explains the observation that selective perimetry provides early detection of ophthalmic and neuro-ophthalmic disease.[5] By extension, it is reasonable to suppose that such tests might therefore better demonstrate the possible ameliorative effects of emerging therapies by detecting them earlier (i.e., when they would not be evident using standard perimetric paradigms).

Although automated perimeters have been in use for more than three decades, our understanding of the mechanisms determining sensitivity to Goldmann size III-V targets under clinical conditions is primarily derived from trials using three *macaca mulatta*.[6] In macaques, photopic and mesopic perimetric sensitivity is mediated by a combination of opponent M- versus L-cone, nonopponent M+L-cone, and S-cone mechanisms, with the relative contribution depending on the size and wavelength of the target.[7] Analogous information pertaining to human subjects is unavailable: this is principally because of the onerous nature of acquiring such data.[8] The early perimetric literature in humans subjects suggests that the rods and cones are approximately equally sensitive to broadband white targets presented on broadband white backgrounds at 1.3 cd.m^{-2}.[7] However, more recent studies using two-color stimulus techniques (one short- and one long-wavelength target), which in effect represent a minimalist approach to determining spectral sensitivity, suggest that the cones may predominantly determine mesopic sensitivity for size III targets (Crossland MD, et al. *IOVS*. 2012;53:ARVO E-Abstract 4822). There is evidence from dark adaptation experiments that scotopic targets are detected by rods peripherally and by a combination of rods and cones at fixation.[4] Results from the two-color technique suggest that paracentral targets may also be detected by a combination of rods and cones (Crossland MD, et al. *IOVS*. 2012;53:ARVO E-Abstract 4822).

There is thus uncertainty regarding the physiological substrate of perimetric target detection in humans under photopic, mesopic, and to a lesser extent scotopic, lighting conditions. We therefore aimed to measure topographical scotopic, mesopic, and photopic spectral sensitivity functions in order to identify the photoreceptor and postreceptoral mechanisms mediating perimetric sensitivity under these conditions. Moreover, we aimed to use our results to predict photoreceptor mechanism isolations for different background and stimulus combinations as a means of aiding the interpretation and design of selective perimetric tests.

Materials and Methods

Three fit and healthy color-normal (as assessed by the Ishihara Plate Test and Farnsworth Munsell 100-Hue) adult male subjects with no history of ocular disease or systemic disease known to affect vision and aged 32 to 41 years were recruited to perform this investigation, which conformed to the tenets of the Declaration of Helsinki. All experiments were conducted using a modified Humphrey 640 perimeter (Humphrey Instruments, San Leandro, CA). Tests were conducted under scotopic, mesopic, and photopic conditions (standard Humphrey white background, luminance 1.3 and 10 cd.m^{-2}; approximate retinal illuminance 1.3 and 2.1 log Td respectively for mesopic and photopic conditions).[9] Subjects were preadapted for 5, 20, and 40 minutes for photopic, mesopic, and scotopic conditions, respectively. Sensitivity was determined using a "full threshold" paradigm[10] for size III and V targets (0.4° and 1.7° diameter, respectively) under photopic and mesopic conditions and for size V targets under scotopic conditions. Stimulus duration was 200 msec and the typical interstimulus interval was 1 to 3 seconds (Patella VM, personal communication, 2015). The stimulus color was controlled by interposing filters in the pathway of the stimulus

projection mechanism: filters with half-bandwidths of 10 nm with peak transmissions at 410, 440, 480, 520, 560, 600, 640, and 680 nm were used. Additionally, a 2 log unit neutral density filter was used to extend the instrument's dynamic range. In order to derive topographical spectral sensitivity curves for subjects, we measured sensitivity at 17 locations: [0°, 0°], [±3°, ±3°], [±9°, ±9°], [±15°, ±15°], [±21°, ±21°] (azimuth, elevation) in one eye using each of the stimulus wavelengths. These locations were chosen as they correspond to locations sampled in the 30-2 field test and although completion of the test protocol required highly motivated observers to perform the more than 17,000 stimulus judgements required, the task was less onerous than that described in simians.[6] The order of testing with respect to wavelength was randomized and two field tests were performed for each subject for each stimulus and background condition. The system was calibrated with a Pritchard 670 telespectroradiometer (Photo Research Inc., Chatsworth, CA). Data for each subject were corrected for absorption by the crystalline lens via a procedure developed by van Norren and Vos[11] and described in detail previously.[12] Corrections for macular pigment density at the point of fixation were made via a psychophysical method. Briefly, sensitivity estimates for the 440-nm stimulus were compared with those for the 520-nm stimulus at the point of fixation and at [±9°, ±9°], making the assumption that the same mechanism was governing threshold at each location (i.e., rods for scotopic conditions, cones for photopic conditions). The depression in sensitivity to the 440-nm stimulus relative to the 520-nm stimulus at the point of fixation was assumed to occur secondary to absorption by the macular pigment: this value was then used to make individual adjustments to the macular pigment optical density template of Stockman and colleagues.[13]

Data at each perimetric location were averaged[6] and fitted with combinations of rod or S-cone, a nonopponent M+L-cone, and an opponent M- versus L-cone spectral sensitivity function. In order to generate templates for fitting, Lamb's photopigment template equation (Equation 1)[14] was used:

$$S(\lambda) = \left(\exp\left(a \times \left(A - {}^{\lambda}\!/_{\lambda_{\max}}\right)\right) + \exp\left(b \times \left(B - {}^{\lambda}\!/_{\lambda_{\max}}\right)\right) + \exp\left(c \times \left(C - {}^{\lambda}\!/_{\lambda_{\max}}\right)\right) + D\right)^{-1} \quad (1)$$

where $a = 70$; $b = 28.5$; $c = -14.1$; $A = 0.880$; $B = 0.924$; $C = 1.104$; $D = 0.655$, with λ_{max} set to 419, 531, and 561 nm for the S-, M-, and L-cone photopigments, respectively, and to 496 nm for rhodopsin.[15,16] Photopigment spectra were then converted to photoreceptor sensitivities using the equation:

$$\text{Photoreceptor sensitivity} = 1 - 10^{\left(-\text{OD} \times S(\lambda)\right)} \quad (2)$$

where OD is the optical density of the photopigment: this was set to 0.4 for the M- and L-cones and to 0.3 for the S-cones and rods (no adjustment for individual variations in optical density were made; see Figure A1). Generated cone spectra were then fitted to spectral sensitivity data using vector combinations[17,18] of an S-cone sensitivity curve, an opponent M- versus L-cone sensitivity curve,[19] a combined M+L-cone nonopponent sensitivity curve, and a rod sensitivity curve:

$$\text{M vs. L} - \text{cone opponent} = \text{abs}(k_1 \times LCS - k_2 \times MCS) \quad (3)$$

$$\text{M} + \text{L} - \text{cone non} - \text{opponent} = k_3 \times LCS + k_4 \times MCS \quad (4)$$

$$\text{S} - \text{cone} = k_5 \times SCS \quad (5)$$

$$\text{Rod sensitivity} = s_1 \times RS \quad (6)$$

where k_1, k_2, k_3, k_4, k_5, and s_1 are scaling constants, LCS is L-cone sensitivity, MCS is M-cone sensitivity, SCS is S-cone sensitivity, and RS is rod sensitivity.[6]

Templates were fitted using the Levenberg-Marquardt algorithm with instrumental weighting as implemented in QtiPlot version 0.9.9[20]: corrected R^2 values were used to determine the best-fitting model. At each stimulus location the relative light absorption for equiquantal targets was calculated in order to illustrate the topographical variation in relative sensitivity of detecting mechanisms. The difference in calculated sensitivity for targets at specified wavelengths was also calculated as "isolation" (if, for example, the rods are 28 dB more sensitive to a stimulus than the M+L-cone mechanism, then the isolation of the rods is 28 dB). Mechanism isolations were calculated for each of the stimulus wavelengths employed at each location in order to facilitate comparisons between previously described methods and to aid in the design of possible future selective perimetric tests.

Results

Intertest sensitivities at each location for each condition were consistent to less than or equal to 3 dB

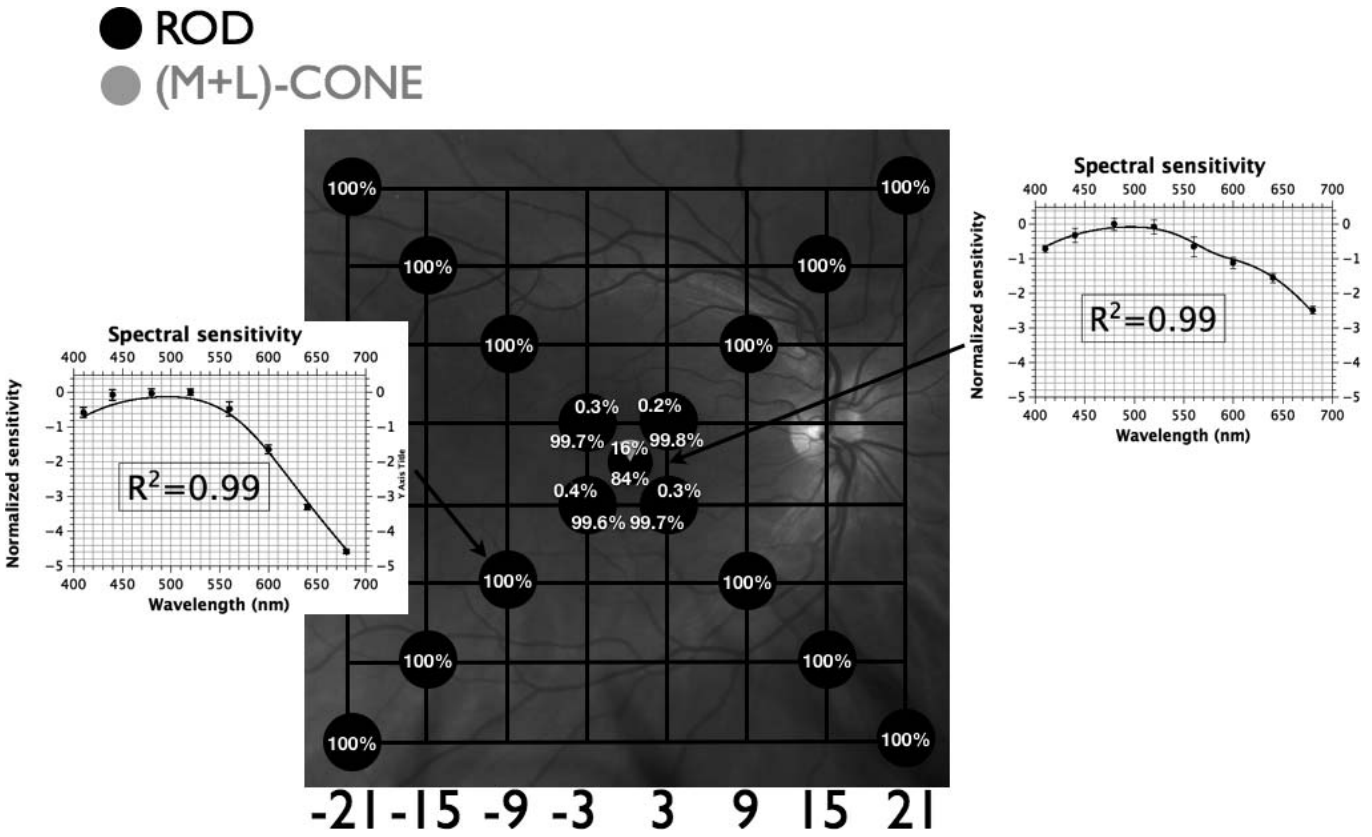

FIGURE 1. Fundus projection of differential sensitivities of rod and cone mechanisms under scotopic conditions. Gridlines are separated by 6°; each circle represents the fundus-projected location in the visual field; relative quantal catches for an equiquantal stimulus incident on the photoreceptor layer are depicted by pie charts at each location (*black* corresponds to absorption by rods; *gray* to absorption by M+L-cones); *insets* demonstrate spectral sensitivity (mean of 3 observers ± SEM) with best-fitting template combinations (see text) and their adjusted R^2 values. Targets at peripheral locations are detected by rods while targets at fixation, and to a lesser extent at [±3°, ±3°], are detected by a combination of rods and (M+L)-cones.

for each subject. The scotopic visual field displayed a deep central depression (>10 dB) at short wavelengths consistent with the known rod-free zone (Figure A2).[21] Peripheral sensitivity was rod-dependent, while cones contributed to central and paracentral sensitivity (Fig. 1). The visual field under mesopic conditions displayed a more modest central depression at short wavelengths, consistent with absorption of short wavelengths by macular pigment/detection by the S-cone mechanism. For targets greater than or equal to 520 nm, the mesopic field had a central peak (Fig. A3). Spectral sensitivity estimates for both size III and V targets suggest that sensitivity at and around fixation was determined by a combination of S-cones and M+L-cones, while for more peripheral locations sensitivity was determined by rods and M+L-cones (Figs. 2A, 2B). The photopic visual field demonstrated a central depression at short wavelengths; this was of similar magnitude to that observed under mesopic conditions and is again consistent with absorption of short wavelengths by macular pigment/detection by the S-cone mechanism. A central peak was observed for targets greater than or equal to 520 nm (Fig. A4). For the size III and size V stimulus conditions (Figs. 3A, 3B), targets were detected by a combination of S-cones, a nonopponent M+L-cone, and an opponent M- versus L-cone mechanism at fixation and by the S-cones and nonopponent M+L-cone mechanism beyond fixation (except at [–3°, +3°] for Goldmann size V targets; Fig. 3B). As outlined above, we also calculated mechanism isolations for different stimulus wavelengths for each background condition to aid in the design and interpretation of selective perimetric tests (see Tables 1–3).

The average macular pigment optical density for centrally presented targets at 480 nm for our subjects was 0.2 (range, 0.1–0.3) under scotopic conditions and 0.7 (range, 0.5–1.0) under photopic conditions. The difference in estimates reflects the fact that macular

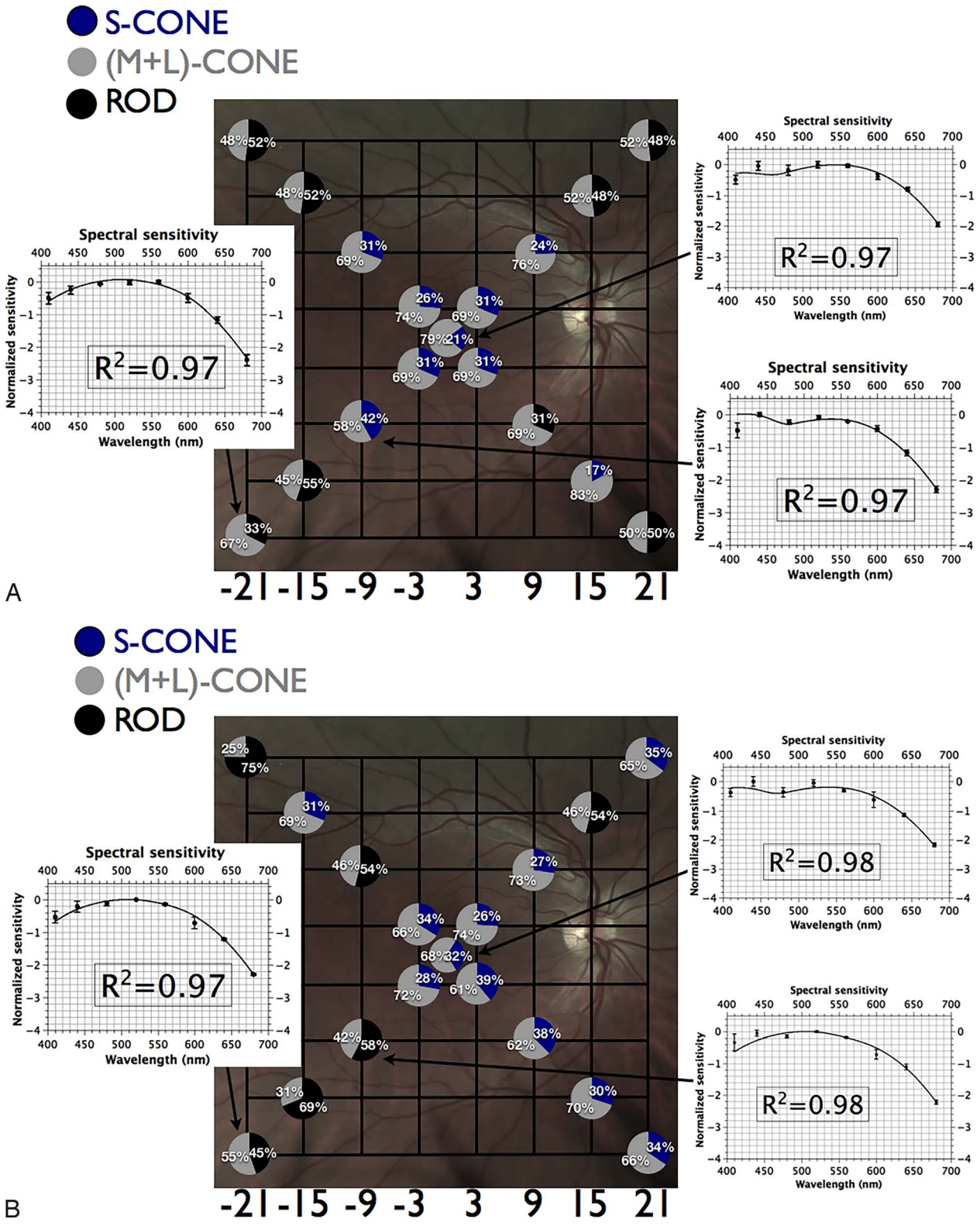

FIGURE 2. (A) Fundus projection of differential rod and cone mechanism sensitivities to size III targets under mesopic conditions. Gridlines are separated by 6°; each *circle* represents the fundus-projected location in the visual field; relative quantal catches for white stimulus incident on the photoreceptor layer (see Appendix) are depicted by pie charts at each location (*black* corresponds to absorption by rods; *blue* corresponds to S-cones; *gray* to absorption by (M+L)-cones); *insets* demonstrate spectral sensitivity (mean of three observers ± SEM)

with best-fitting template combinations (see text) and their adjusted R^2 values. Targets at peripheral locations are detected by rods and (M+L)-cones while more central targets are detected by a combination of S-cones and (M+L)-cones. (B) Fundus projection of differential rod and cone mechanism sensitivities to size V targets under mesopic conditions. Gridlines are separated by 6°; each *circle* represents the fundus-projected location in the visual field; relative quantal catches for white stimulus incident on the photoreceptor layer (see Appendix) are depicted by pie charts at each location (*black* corresponds to absorption by rods; *blue* corresponds to S-cones; *gray* to absorption by (M+L)-cones); *insets* demonstrate spectral sensitivity (mean of three observers ± SEM) with best-fitting template combinations (see text) and their adjusted R^2 values. Targets at peripheral locations are detected by rods and (M+L)-cones while more central targets are detected by a combination of S-cones and (M+L)-cones.

pigment density declines with eccentricity (density estimates under rod-isolating conditions exclude the central fovea and are therefore anticipated to be lower than under photopic conditions). The average scaling constant for the crystalline lens optical density was 1.15 (range, 1.08–1.20).[11]

Discussion

Our study seeks to elucidate perimetric spectral sensitivity under scotopic, mesopic, and photopic conditions and to further identify the receptoral/postreceptoral mechanisms governing target detection. General limitations of our study include the fact that we assumed "normal" peak sensitivities and optical densities for the photopigments of our observers. Furthermore, there remains uncertainty regarding the way in which signals from different pathways are combined by the visual system and whilst the vector combination[17,18] we used may better reflect this combination than other models, it may still be imperfect.

As anticipated, scotopic peripheral visual function is rod dominated ($\geq$ 28 ± 2 dB of isolation from M+L-cones at $\leq$ 480 nm). At fixation, and to a lesser extent at [±3°, ±3°], participation of the M+L-cone mechanism was evident (rod isolation 11 ± 1 dB centrally and $\geq$ 28 ± 2 dB peripherally at $\leq$480 nm; see Fig. 1, Table 1). As only two mechanisms are active, the established practice of two-color scotopic perimetry[4] to distinguish rod from cone, or mixed rod/cone, detection appears to be superficially sound; however, it is not uncommon for S-cone intrusion to occur in retinitis pigmentosa.[22] This would be incorrectly interpreted as mixed-rod/cone detection unless more extensive spectral sensitivity measurements were made.

Under mesopic conditions, size III and V targets appeared to be detected by S-cones and the M+L-cone mechanism at, and close to, fixation while at more peripheral locations detection was mediated by rods and a nonopponent M+L-mechanism. Mesopic testing therefore appears to maximize the redundancy of target detection; this has two important sequelae. First, identification of those mechanisms governing perimetric sensitivity is complex, as short wavelength targets may be detected by either S-cones or rods. Thus, testing with short-wavelength targets under mesopic conditions may not provide unambiguous information unless such testing forms part of a more detailed spectral sensitivity assessment. Second, this redundancy in target detection is anticipated to result in insensitivity in identifying functional deficits secondary to pathology, and may indeed account for the early observation that mesopic sensitivity for achromatic targets is resilient to isolated losses of cone or rod function.[7] Accordingly, we suggest that testing under scotopic and photopic conditions is preferable if broadband white stimuli are to be used. Furthermore, our results suggest that if mesopic testing is employed, long wavelength targets ($\geq$ 640 nm, which provide $\geq$ 17 ± 3 dB of M+L-cone isolation; see Table 2) are preferable to broadband white stimuli.

Under photopic conditions, sensitivity at the point of fixation for Goldmann size III and V targets was best modeled by a combination of S-cones, a nonopponent M+L-cone mechanism, and an opponent M- versus L-cone mechanism. These data are consistent with previous observations for centrally presented targets[23] and with simian data.[6] Spectral sensitivities at more peripheral locations were best described by a vector combination of S-cones and a nonopponent M+L-cone mechanism; this finding is in contrast to the psychophysical findings of Harwerth et al.[6] in the macaque, who found evidence for participation of the M- versus L-cone opponent mechanism at most stimulus locations using the same background conditions as ours. Several factors may account for this discrepancy: first, our results may reflect a physiological difference between the human visual system and that of *macaca mulatta*. For example, it is known that the retinal illuminance for the same light source is higher in the macaque than the human[24] (this fact would favor color-opponent mechanisms) and there may be differences in the

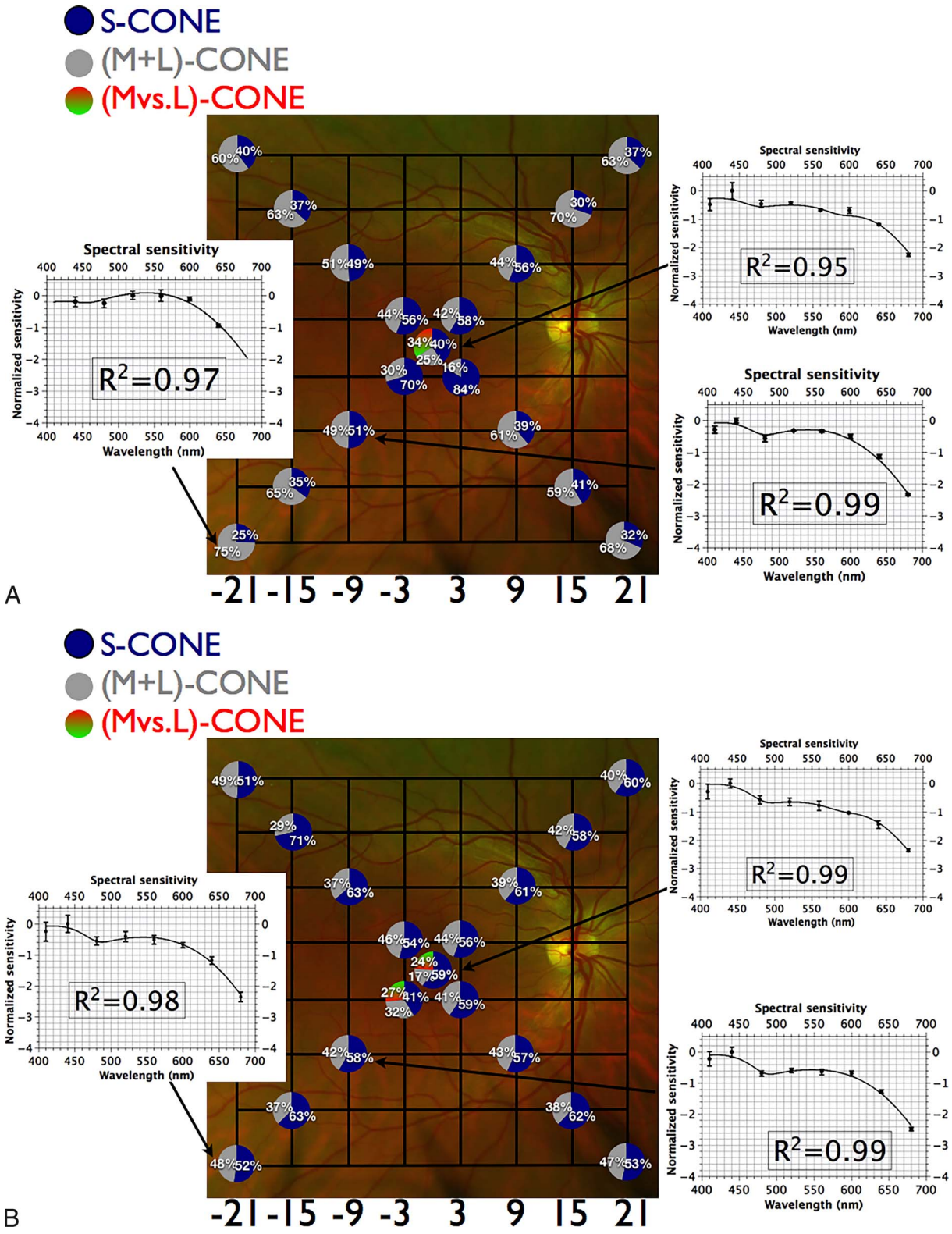

FIGURE 3. (A) Fundus projection of differential sensitivities to size III targets under photopic conditions. Gridlines are separated by 6°; each *circle* represents the fundus-projected location in the visual field; relative quantal catches for white stimulus incident on the photoreceptor layer (see Appendix) are depicted by pie charts at each location (*blue* corresponds to S-cones; *gray* to absorption by [M+L]-cones; *green*-red to absorption by the [M versus L]-cone mechanism); *insets* demonstrate spectral sensitivity (mean of 3 observers

± SEM) with best-fitting template combinations (see text) and their adjusted R^2 values. Targets at peripheral locations are detected by S-cones and (M+L)-cones whilst targets at fixation are detected by a combination of S-cones, a nonopponent (M+L)-cone and an opponent (M versus L)-cone mechanism. (B) Fundus projection of differential sensitivities to size V targets under photopic conditions. *Gridlines* are separated by 6°; each *circle* represents the fundus-projected location in the visual field; relative quantal catches for white stimulus incident on the photoreceptor layer (see Appendix) are depicted by pie charts at each location (*blue* corresponds to S-cones; *gray* to absorption by [M+L]-cones; *green-red* to absorption by the [M versus L]-cone mechanism); *insets* demonstrate spectral sensitivity (mean of 3 observers ± SEM) with best-fitting template combinations (see text) and adjusted R^2 values. Targets at peripheral locations are detected by S-cones and (M+L)-cones while targets at fixation are detected by a combination of S-cones, a nonopponent (M+L)-cone and an opponent (M versus L)-cone mechanism.

gains, spatial, and temporal summation properties of the opponent and nonopponent mechanisms between species. Second, our data were modeled using a vector combination of mechanisms[17,18] and quantal data,[25] while Harwerth et al.[6] used energy data for analysis and assumed that the spectral sensitivity function represented an upper envelope of the component functions. It is also important to note that even when Harwerth et al.'s[6] data and analysis supported detection via the opponent M- versus L-cone mechanism, the "isolation" of this mechanism from the nonopponent mechanism was poor. Finally, it is also important to note that our findings are in keeping with physiological recordings from macaque retinal ganglion cells using size III stimuli, which demonstrate that M-cells are preferentially activated by such stimuli in conventional (white-on-white) perimetry.[26] Our findings would also suggest limitations to the general applicability of Harwerth et al.'s[6] data to the human visual system.[8]

Our photopic data suggest that neither central or peripheral sensitivity for 200-msec targets presented on a 10-cd.m^{-2} background are well-described by the CIE $V_{(\lambda)}$ function; these observations are in agreement with previous studies of peripheral sensitivity[27] and with estimates of central sensitivity under similar conditions.[28] This phenomenon is partially explained by considering the postreceptoral pathways involved in target detection. The brightness-matching paradigm used to derive the $V_{(\lambda)}$ function uses a flickering stimulus (25 Hz in the most recent update of the CIE function).[25] This is likely to favor the parasol ganglion cell pathway and other pathways with robust responses to flickering stimuli such as the smooth monostratified cells,[29] while the stimulus used in the Humphrey perimeter is more likely to enable other pathways, such as the S-cone pathway and the midget cell pathway[30] (which have poorer temporal sensitivity), to have some participation in target detection. Furthermore, increased peripheral sensitivity to short wavelength targets reflects the distribution of S-cones.[31]

Although the use of short wavelength targets presented on 10 cd.m^{-2} broadband white back-

Table 1. Photoreceptor Mechanism Isolation by Wavelength for Scotopic Conditions

Target Wavelength	Isolation: Receptor Type	Magnitude of Isolation (Mean ± SEM)		
		Periphery	[±3°, ±3°]	Fixation
410 nm	Rods	≥36 ± 2 dB	33 ± 2 dB	16 ± 1 dB
440 nm	Rods	≥34 ± 2 dB	31 ± 2 dB	14 ± 1 dB
480 nm	Rods	≥31 ± 2 dB	28 ± 2 dB	11 ± 1 dB
520 nm	Rods	≥28 ± 2 dB	25 ± 2 dB	8 ± 1 dB
560 nm	Rods	≥22 ± 2 dB	19 ± 2 dB	2 ± 1 dB
600 nm	Rods (M+L-cones at fixation)	≥13 ± 2 dB	10 ± 2 dB	−7 ± 1 dB (i.e., M+L-cones isolated)
640 nm	Rods (M+L-cones at fixation)	≥3 ± 2 dB	0 ± 2 dB	−17 dB ± 1 (i.e., M+L-cones isolated)
680 nm	Rods (M+L-cones at fixation & [±3°, ±3°])	>0 ± 2 dB	−3 ± 2 dB (i.e., M+L-cones isolated)	−20 dB ± 1 (i.e., M+L-cones isolated)

Difference in sensitivity (dB) calculated from vector curve fitting of mechanism templates. Positive values represent isolation of the rods from the M+L-cones and negative values vice versa.

Table 2. Photoreceptor Mechanism Isolation by Wavelength for Mesopic Conditions

	Isolation: Receptor Type		Magnitude of Isolation (Mean ± SEM)	
Target Wavelength	Size III	Size V	Size III	Size V
410 nm	Rods/S-cones	Rods/S-cones	NA	NA
440 nm	Rods/S-cones	Rods/S-cones	NA	NA
480 nm	Rods/S-cones	Rods/S-cones	NA	NA
520 nm	M+L-cones	Rods/S-cones	>0 dB	NA
560 nm	M+L-cones	M+L-cones	≥5 ± 2 dB	≥2 ± 3 dB
600 nm	M+L-cones	M+L-cones	≥13 ± 2 dB	≥10 ± 3 dB
640 nm	M+L-cones	M+L-cones	≥20 ± 2 dB	≥17 ± 3 dB
680 nm	M+L-cones	M+L-cones	≥23 ± 2 dB	≥20 ± 3 dB

Difference in sensitivity (dB) calculated from vector curve fitting of mechanism templates. Short wavelength targets may be detected by either rods or S-cones and testing with such targets is not recommended for clinical purposes unless it forms part of a more detailed spectral sensitivity assessment (see main article text).

grounds for the isolation of the S-cone mechanism has been described,[32] the degree of isolation achieved (≥9 ± 1 dB for a 440 nm size V stimulus) is less than that previously reported for the more commonly employed yellow backgrounds at 100 cd.m^{-2} (i.e., the background condition typically used in so-called short wavelength automated perimetry).[33] A broadband white 10 cd.m^{-2} background condition is therefore not recommended for isolation of the S-cone mechanism for clinical testing. Stimuli at greater than or equal to 640 nm, as used in some previous investigations,[34] would be anticipated to provide greater than or equal to 20 ± 2 dB of M+L-cone isolation (assuming that the minimum isolation is at least on par with that for size III targets under mesopic conditions; see Table 3) and are therefore appropriate for clinical testing. However, for reasons elaborated above, the two-color technique may provide erroneous information about rod intrusion under photopic conditions: full identification of the active mechanisms may therefore require testing with more stimulus wavelengths.[22]

Acknowledgments

Supported by grants from the Bayer Global Ophthalmology Awards Program (MPS), the RANZCO Eye Foundation (Novartis/RANZCO Scholarship: MPS) and the NIHR Biomedical Research Centres of Oxford University Hospitals (REM) & Moorfields Eye Hospital NHS Foundation Trust (REM, ATM).

Table 3. Photoreceptor Mechanism Isolation by Wavelength for Photopic Conditions in the Periphery

	Isolation Receptor Type		Magnitude of Isolation (Mean ± SEM)	
Target Wavelength	Size III	Size V	Size III	Size V
410 nm	S-cones	S-cone	≥11 ± 4 dB	≥14 ± 1 dB
440 nm	S-cone	S-cones	≥5 ± 4 dB	≥9 ± 1 dB
480 nm	M+L-cones	M+L-cones	≥5 ± 4 dB	≥1 ± 1 dB
520 nm	M+L-cones	M+L-cones	≥22 ± 4 dB	≥18 ± 1 dB
560 nm	M+L-cones	M+L-cones	≥39 ± 4 dB	≥35 ± 1 dB
600 nm	M+L-cones	M+L-cones	≥52 ± 4 dB	≥48 ± 1 dB
640 nm	M+L-cones	M+L-cones	≥60 ± 4 dB	≥56 ± 1 dB
680 nm	M+L-cones	M+L-cones	≥61 ± 4 dB	≥57 ± 1 dB

Difference in sensitivity (dB) calculated from vector curve fitting of mechanism templates. Values ≤ 480 nm refer to S-cone mechanism isolation from the M+L-cone mechanism, while values > 480 nm refer to M+L-cone mechanism isolation from S-cones. Estimates of M+L-cone mechanism isolation can be conservatively estimated from values for size III targets under mesopic conditions.

References

1. Henson DB. *Visual Fields*. 2nd ed. Oxford: Butterworth-Heinemann; 2000.
2. Acton JH, Greenstein VC. Fundus-driven perimetry (microperimetry) compared to conventional static automated perimetry: similarities, differences, and clinical applications. *Can J Ophthalmol*. 2013;48:358–363.
3. MacLaren RE, Groppe M, Barnard AR, et al. Retinal gene therapy in patients with choroideremia: initial findings from a phase 1/2 clinical trial. *Lancet*. 2014;383:1129–1137.
4. Jacobson SG, Voigt WJ, Parel JM, et al. Automated light- and dark-adapted perimetry for evaluating retinitis pigmentosa. *Ophthalmology*. 1986;93:1604–1611.
5. Johnson CA. Selective versus nonselective losses in glaucoma. *J Glaucoma*. 1994;3(suppl 1):S32–S44.
6. Harwerth RS, Smith EL III, DeSantis L. Mechanisms mediating visual detection in static perimetry. *Invest Ophthalmol Vis Sci*. 1993;34:3011–3023.
7. Sloan LL. The Tubinger perimeter of Harms and Aulhorn. Recommended procedures and supplementary equipment. *Arch Ophthalmol*. 1971;86:612–622.
8. Johnson CA, Marshall D Jr. Aging effects for opponent mechanisms in the central visual field. *Optom Vis Sci*. 1995;72:75–82.
9. Wyszecki GW, Stiles WS. *Color science*. New York: John Wiley & Sons; 1982.
10. Simunovic MP, Regan BC, Mollon JD. Is color vision deficiency an advantage under scotopic conditions? *Invest Ophthalmol Vis Sci*. 2001;42:3357–3364.
11. Norren DV, Vos JJ. Spectral transmission of the human ocular media. *Vision Res*. 1974;14:1237–1244.
12. Simunovic MP, Cullerne A, Colley A, Wilson TD. How well does color perimetry isolate responses from individual cone mechanisms? *J Glaucoma*. 2004;13:22–27.
13. Stockman A, Sharpe LT, Fach C. The spectral sensitivity of the human short-wavelength sensitive cones derived from thresholds and color matches. *Vision Res*. 1999;39:2901–2927.
14. Lamb TD. Photoreceptor spectral sensitivities: common shape in the long-wavelength region. *Vision Res*. 1995;35:3083–3091.
15. Dartnall HJ, Bowmaker JK, Mollon JD. Human visual pigments: microspectrophotometric results from the eyes of seven persons. *Proc R Soc Lond B Biol Sci*. 1983;220:115–130.
16. Thomas PB, Mollon JD. Modelling the Rayleigh match. *Vis Neurosci*. 2004;21:477–482.
17. Ingling CR Jr, Huong-Peng-Tsou B. Orthogonal combination of the three visual channels. *Vision Res*. 1977;17:1075–1082.
18. Kremers J, Meierkord S. Rod-cone-interactions in deuteranopic observers: models and dynamics. *Vision Res*. 1999;39:3372–3385.
19. Thornton JE, Pugh EN Jr. Red/Green color opponency at detection threshold. *Science*. 1983;219:191–193.
20. Nocedal J, Wright SJ. *Numerical Optimization*. New York: Springer-Verlag; 1999.
21. Ahnelt PK. The photoreceptor mosaic. *Eye (Lond)*. 1998;12(pt 3b):531–540.
22. Massof RW, Johnson MA, Finkelstein D. Peripheral absolute threshold spectral sensitivity in retinitis pigmentosa. *Br J Ophthalmol*. 1981;65:112–121.
23. Pokorny J, Smith VC, Verriest G, Pinckers AJLG. *Congenital and Acquired Color Vision Defects*. New York: Grune & Stratton; 1979.
24. Lee BB, Pokorny J, Smith VC, Martin PR, Valberg A. Luminance and chromatic modulation sensitivity of macaque ganglion cells and human observers. *J Opt Soc Am A*. 1990;7:2223–2236.
25. Sharpe LT, Stockman A, Jagla W, Jagle H. A luminous efficiency function, V*(lambda), for daylight adaptation. *J Vis*. 2005;5(11):948–968.
26. Swanson WH, Sun H, Lee BB, Cao D. Responses of primate retinal ganglion cells to perimetric stimuli. *Invest Ophthalmol Vis Sci*. 2011;52:764–771.
27. Weale RA. Spectral sensitivity and wave-length discrimination of the peripheral retina. *J Physiol*. 1953;119:170–190.
28. Verriest G, Uvijls A. Spectral increment thresholds on a white background in different age groups of normal subjects and in acquired ocular diseases. *Doc Ophthalmol*. 1977;43:217–248.
29. Crook JD, Peterson BB, Packer OS, et al. The smooth monostratified ganglion cell: evidence for spatial diversity in the Y-cell pathway to the lateral geniculate nucleus and superior colliculus in the macaque monkey. *J Neurosci*. 2008;28:12654–12671.
30. Solomon SG, Lennie P. The machinery of colour vision. *Nat Rev Neurosci*. 2007;8:276–286.
31. Calkins DJ. Seeing with S cones. *Prog Retin Eye Res*. 2001;20:255–287.
32. Jacobson SG, Marmor MF, Kemp CM, Knighton RW. SWS (blue) cone hypersensitivity in a newly identified retinal degeneration. *Invest Ophthalmol Vis Sci*. 1990;31:827–838.
33. Sample PA, Johnson CA, Haegerstrom-Portnoy G, Adams AJ. Optimum parameters for short-wavelength automated perimetry. *J Glaucoma*. 1996;5:375–383.
34. Zele AJ, Dang TM, O'Loughlin RK, Guymer RH, Harper A, Vingrys AJ. Adaptation mechanisms, eccentricity profiles, and clinical implementation of red-on-white perimetry. *Optom Vis Sci*. 2008;85:309–317.

Appendix

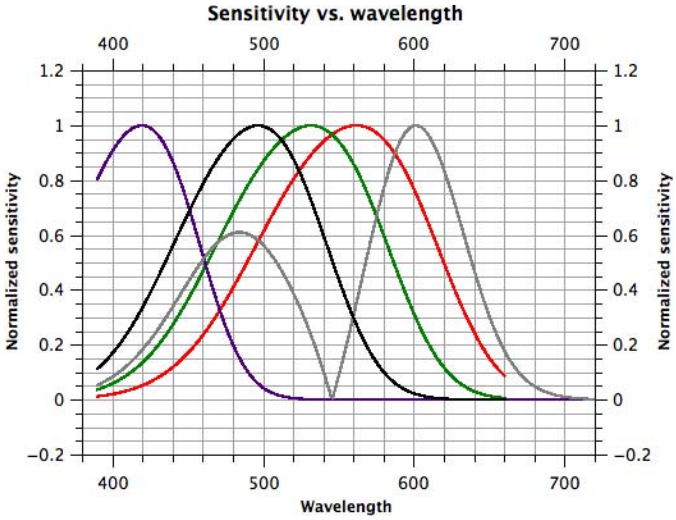

FIGURE A1. Spectral sensitivity of generated photoreceptor/post-receptoral mechanism templates. S-cones are represented by a *violet line*, M-cones by a *dark green line*, L-cones by a *red line*, rods by a *black line* and the M- versus L-mechanism by a *gray line*.

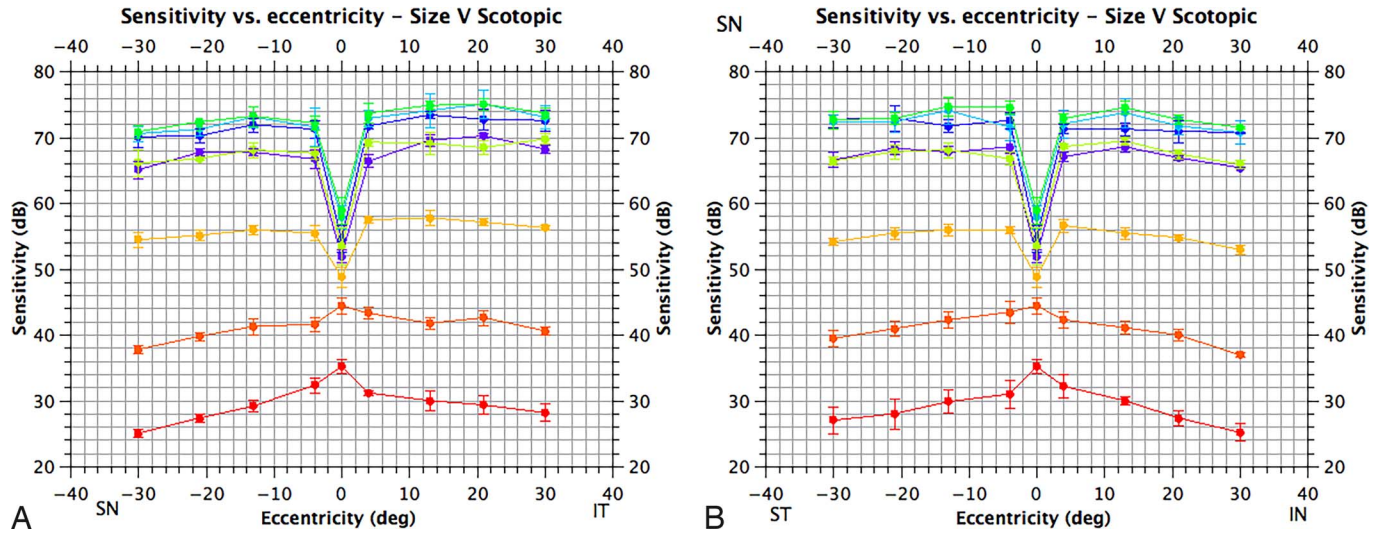

FIGURE A2. Scotopic visual fields for size V targets. The horizontal axis corresponds to eccentricity and the vertical to sensitivity in dB (adjusted for crystalline lens absorption). (A) Sensitivity along a superonasal to inferotemporal axis and (B) along a superotemporal to inferonasal axis (of the visual field). Sensitivity for different targets is color-coded; 410 nm, *violet*; 440 nm, *blue*; 480 nm, *blue-green*; 520 nm, *green*; 560 nm, *yellow-green*; 600 nm, *orange*; 640 nm, *orange-red*; 680 nm, *red*. Means are plotted as *filled circles* with standard errors as bars ($N = 3$).

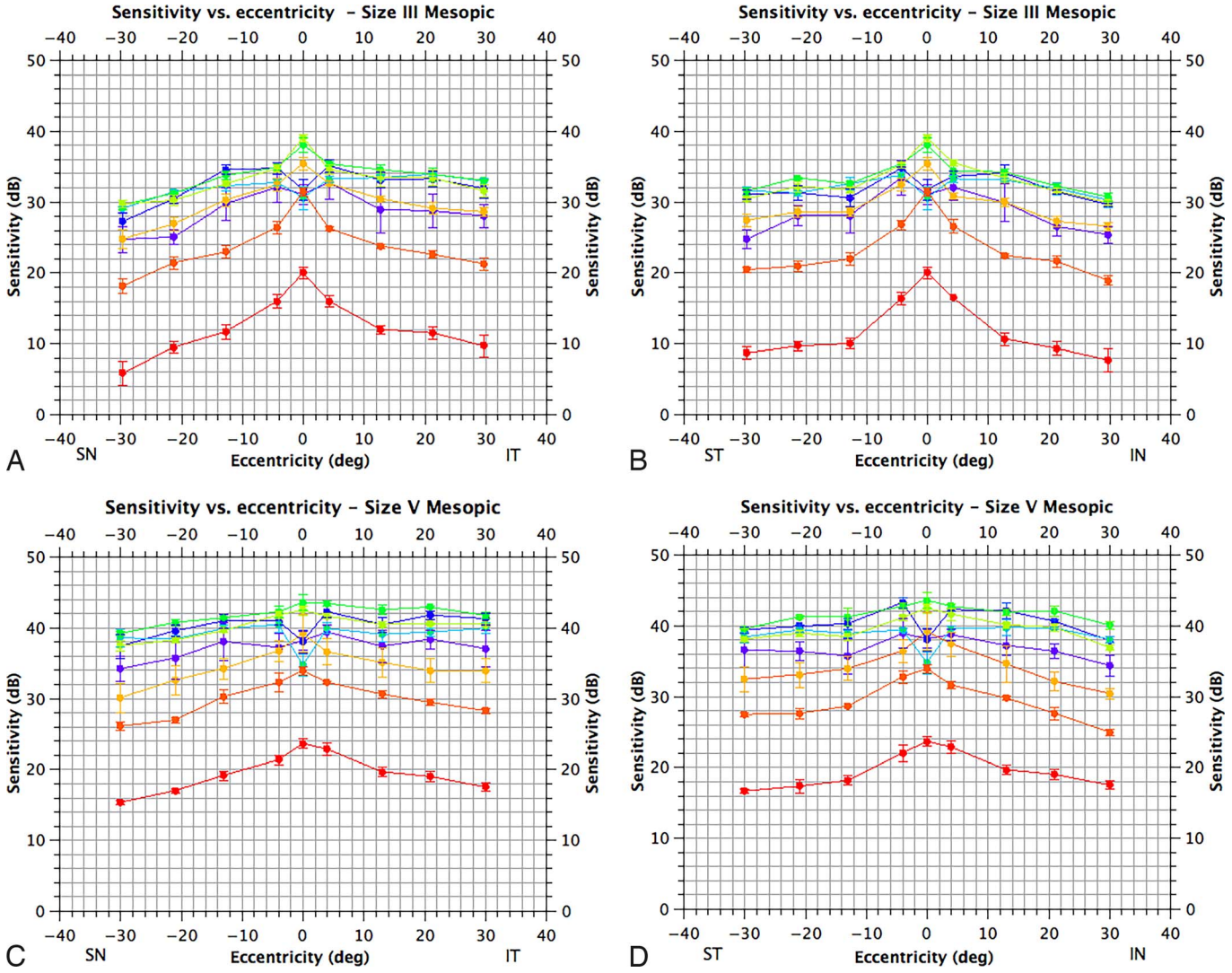

FIGURE A3. Mesopic visual fields for size III & V targets. The horizontal axis corresponds to eccentricity and the vertical to sensitivity in decibels (adjusted for crystalline lens absorption). (A) Sensitivity along a superonasal to inferotemporal axis for size III targets; (B) along a superotemporal to inferonasal axis for size III targets; (C) along a superonasal to inferotemporal axis for size V targets; and (D) along a superotemporal to inferonasal axis for size V targets. Locations refer to the visual field. Sensitivity for different targets is color-coded; 410 nm, *violet*; 440 nm, *blue*; 480 nm, *blue-green*; 520 nm, *green*; 560 nm, *yellow-green*; 600 nm, *orange*; 640 nm, *orange-red*; 680 nm, *red*. Means are plotted as *filled circles* with standard errors as bars ($N = 3$).

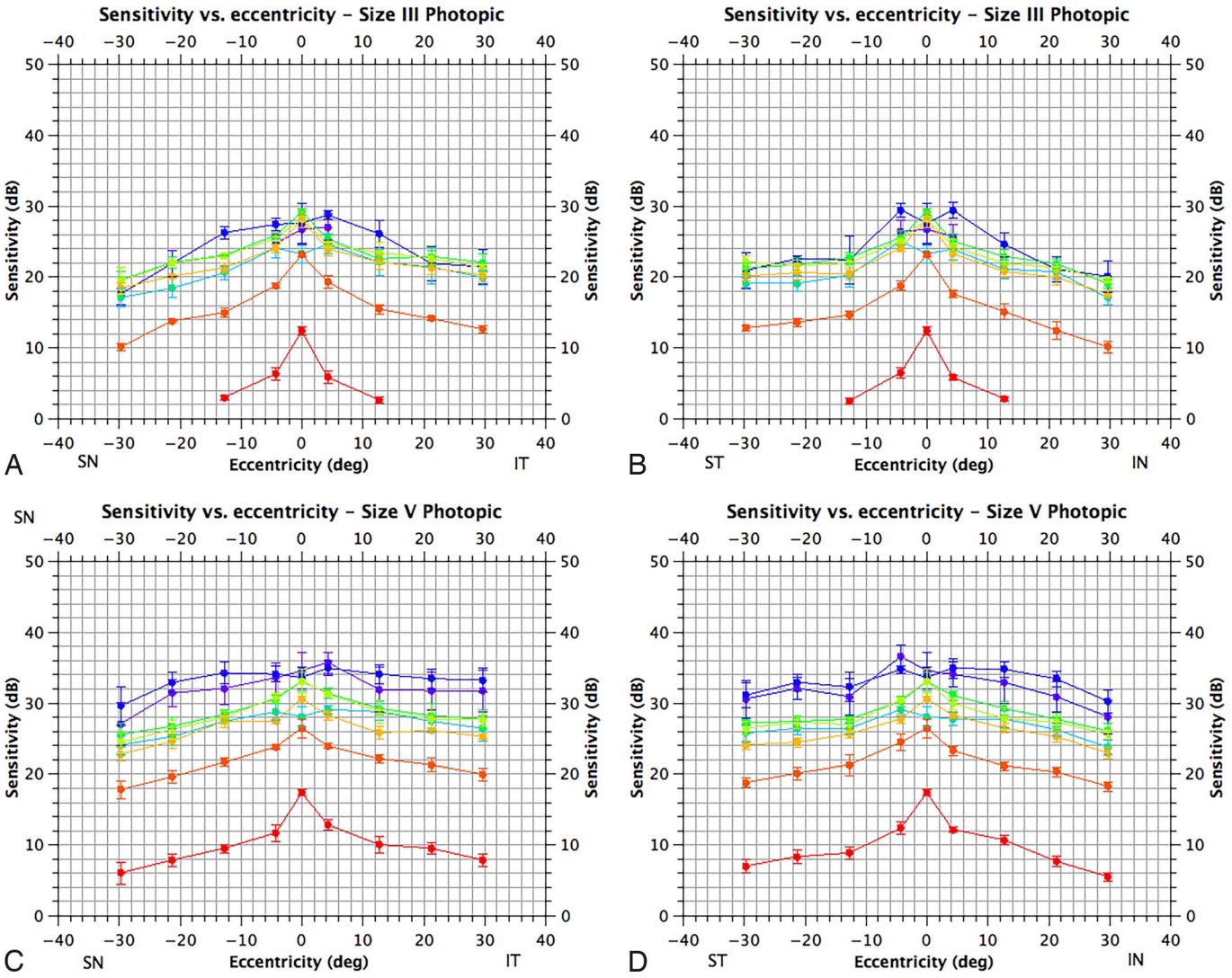

FIGURE A4. Photopic visual fields for size III & V targets. The horizontal axis corresponds to eccentricity and the vertical to sensitivity in decibels (adjusted for crystalline lens absorption). (A) Sensitivity along a superonasal to inferotemporal axis for size III targets; (B) along a superotemporal to inferonasal axis for size III targets; (C) along a superonasal to inferotemporal axis for size V targets and D. along a superotemporal to inferonasal axis for size V targets. Locations refer to the visual field. Sensitivity for different targets is *color-coded*; 410 nm, *violet*; 440 nm, *blue*; 480 nm, *blue-green*; 520 nm, *green*, 560 nm, *yellow-green*; 600 nm, *orange*; 640 nm, *orange-red*; 680 nm, *red*. Means are plotted as *filled circles* with standard errors as bars ($N = 3$).